OXFORD

Social Cognitive and Affective Neuroscience, 2022, **17**, 965–976

DOI: https://doi.org/10.1093/scan/nsac031
Advance Access Publication Date: 21 April 2022
Original Manuscript

The cortical and subcortical correlates of face pareidolia in the macaque brain

Jessica Taubert,[1,2] Susan G. Wardle,[1] Clarissa T. Tardiff,[1] Elissa A. Koele,[1] Susheel Kumar,[1] Adam Messinger,[1] and Leslie G. Ungerleider[1,†]

[1]Laboratory of Brain and Cognition, The National Institute of Mental Health, NIH, Bethesda, MD 20892, USA
[2]School of Psychology, The University of Queensland, Brisbane, QLD 4072, Australia
Correspondence should be addressed to Jessica Taubert, School of Psychology, The University of Queensland, Building 24A, St Lucia, QLD 4067, Australia. E-mail: j.taubert@uq.edu.au.
[†]Passed away suddenly on the 11th of December 2020 after helping to prepare the manuscript for submission with the expectation of senior authorship.

Abstract

Face detection is a foundational social skill for primates. This vital function is thought to be supported by specialized neural mechanisms; however, although several face-selective regions have been identified in both humans and nonhuman primates, there is no consensus about which region(s) are involved in face detection. Here, we used naturally occurring errors of face detection (i.e. objects with illusory facial features referred to as examples of 'face pareidolia') to identify regions of the macaque brain implicated in face detection. Using whole-brain functional magnetic resonance imaging to test awake rhesus macaques, we discovered that a subset of face-selective patches in the inferior temporal cortex, on the lower lateral edge of the superior temporal sulcus, and the amygdala respond more to objects with illusory facial features than matched non-face objects. Multivariate analyses of the data revealed differences in the representation of illusory faces across the functionally defined regions of interest. These differences suggest that the cortical and subcortical face-selective regions contribute uniquely to the detection of facial features. We conclude that face detection is supported by a multiplexed system in the primate brain.

Key words: face pareidolia; face patch system; amygdala; macaque fMRI

Introduction

We detect faces faster than we detect other kinds of visual objects in the environment. Regardless of whether faces are relevant to the task at hand, they summon eye movements (Crouzet *et al.*, 2010), reduce reaction times (Taubert *et al.*, 2011) and interfere with nonface tasks (Fenske and Eastwood, 2003). These markers of involuntary face detection, evident in adult human behavior, are also shared with newborn human infants (Goren *et al.*, 1975; Simpson *et al.*, 2020) and other primate species (Sugita, 2008; Taubert and Parr, 2012; Taubert *et al.*, 2017) and are thought to play a foundational role in the development of social intelligence (de Gelder *et al.*, 2003; Johnson, 2005; Shultz *et al.*, 2018). Yet the neural mechanisms underlying face detection are only partially understood.

Current neural models of primate vision largely attribute face detection to cortical face-selective regions in the inferior temporal cortex (ITC) that can be localized in humans and macaques using functional magnetic resonance imaging (fMRI) (Kanwisher *et al.*, 1997; Tsao *et al.*, 2003). In macaques, these regions form an interconnected network of spatially distinct face patches mostly located along the superior temporal sulcus (STS) (Premereur *et al.*, 2016). Electrophysiological recordings have revealed that neurons within this network respond more strongly to faces than to other kinds of objects (Tsao *et al.*, 2006; Bell *et al.*, 2011; Taubert *et al.*, 2015a,b; Taubert *et al.*, 2018b) and, therefore, face detection has been thought to be the result of activating the face-selective network in the ITC (Tsao and Livingstone, 2008; Taubert *et al.*, 2020a,b).

However, any account that attributes face detection entirely to activity in the ITC cannot explain two key observations in the literature: (i) infant macaques spontaneously orient toward primate faces and, thus, distinguish them from other visual objects before the face-selective network develops during infancy (Sugita, 2008; Livingstone *et al.*, 2017) and (ii) cortically blind patients also spontaneously orient toward faces even though they do not report seeing faces (Morris *et al.*, 2001; Tamietto and de Gelder, 2010). Since the early visual areas in the occipital lobe are thought to be the primary source of information feeding into the ITC (Mishkin *et al.*, 1983; Grimaldi *et al.*, 2016; Pitcher and Ungerleider, 2021), both of these observations suggest that primates are capable of distinguishing faces from non-face objects without activating the cortical face-selective network in a feedforward manner. Although the exact mechanism(s) responsible for this form of involuntary face detection has not been identified, it has been suggested that it is operational at birth, or shortly thereafter, and is broadly tuned to rudimentary face structure that can be

Received: 10 August 2021; **Revised:** 27 March 2022; **Accepted:** 19 April 2022

coarsely matched to any face or face-like configuration in the environment (Goren *et al.*, 1975; Pascalis *et al.*, 2002; Johnson, 2005; Reid *et al.*, 2017).

In addition to the face patches in the ITC, face stimuli are also known to activate other brain areas in the macaque brain, including patches within the prefrontal cortex (PFC) (Tsao *et al.*, 2008) and the amygdala (Hadj-Bouziane *et al.*, 2008). Recently, we have found that amygdala loss eliminates the spontaneous biases toward real and illusory faces in a free viewing task (Taubert *et al.*, 2018a). This finding indicates that the amygdala might also contribute to the detection and prioritization of face stimuli under natural viewing conditions (also see (Gamer *et al.*, 2013). Despite a possible role for the face patches and the amygdala in face detection, their individual contributions to this important task are not yet clear.

Although we detect faces quickly, we often make mistakes and detect faces when none exist. Face pareidolia describes the common perception of illusory facial features on otherwise inanimate objects, such as vegetables. Although recent behavioral studies have shown that illusory facial features confer face-like advantages for objects when testing humans (Omer *et al.*, 2019; Wardle *et al.*, 2020; Alais *et al.*, 2021; Caruana and Seymour, 2022; Keys *et al.*, 2021) and macaques (Taubert *et al.*, 2017) in detection paradigms, we do not know whether illusory faces tap into the specialized face-selective mechanisms in the macaque brain. Therefore, the goal of this study was to determine whether examples of face pareidolia, when presented to awake macaques, evoke the neural signature of face processing using fMRI. In the first experiment, we scanned four macaques while they fixated images of illusory faces and matched non-face objects. We predicted that illusory faces would elicit a greater response than matched objects from face-selective regions of interest (ROIs), i.e. the face patches in the ITC, the amygdala and a face patch in the ventral lateral PFC (known as a face patch in prefrontal cortex (PV)), but not from an object-selective (OS) patch localized in the ITC.

In Experiment 2, we scanned two additional subjects to compare the response of these different brain areas to three stimulus categories (i.e. real faces, illusory faces and matched objects; Wardle *et al.*, 2020). Including real faces in the experimental design provided the opportunity to evaluate the definition of the ROIs and directly compare activity evoked by real faces to activity evoked by illusory faces. We predicted that, like the face-selective regions in the human brain, all the face-selective regions in the macaque brain would respond more selectively to real faces than to illusory faces. Including real faces in the experimental design also enabled us to use multivariate analytical approaches to further probe the neural representation of illusory faces in the ROIs. Since the amygdala is thought to be tuned more broadly than the cortical face-selective patches (Morris *et al.*, 2001; Taubert *et al.*, 2017, 2018a), we expected that the amygdala might encode illusory faces as being more similar to real faces than to matched objects.

Method

Subjects

All the experimental procedures and animal welfare were in full compliance with the Guidelines for the Care and Use of Laboratory Animals by the U.S. National Institutes of Health and approved by the Animal Care and Use Committee of the U.S. National Institutes of Mental Health/National Institute of Health. In total, six male rhesus macaques (*Macaca mulatta*) participated in this study. In Experiment 1, we tested four macaques (9–14 years of age, 7–11.5 kg at the time of testing). Each of these subjects was an experienced fMRI and behavioral participant. Additionally, they had also participated in multiple behavioral studies and training exercises that included examples of illusory faces (Taubert *et al.*, 2017). In Experiment 2, we tested two male rhesus macaques (6 and 7 years of age, weighing between 9.9–11.2 kg at the time of testing).

All six subjects were socially housed in pairs with regular access to large play cages. Each subject was surgically implanted with an MRI-compatible headpost under sterile conditions using isoflurane anesthesia. After recovery, the subjects were slowly acclimated to the experimental procedure.

Echo-planar imaging data acquisition

Before each fMRI scanning session, an exogenous contrast agent [monocrystalline iron oxide nanocolloid (MION)] was injected into the femoral vein to increase the signal-to-noise ratio (Vanduffel *et al.*, 2001). MION doses were determined for each subject (~8–10 mg/kg). Structural and functional data were acquired in a 4.7 T, 60 cm vertical scanner (Bruker Biospec, Ettlingen, Germany) equipped with a Bruker S380 gradient coil. Subjects viewed the visual stimuli projected onto a screen above their head through a mirror positioned in front of their eyes. We collected whole-brain images with a four-channel transmit and receive radiofrequency coil system (Rapid MR International, Columbus, OH, USA). A low-resolution anatomical scan was also acquired in the same session to serve as an anatomical reference [Modified Driven Equilibrium Fourier Transform (MDEFT) sequence, voxel size: 1.5 × 0.5 × 0.5 mm, field of view (FOV): 96 × 48 mm, matrix size: 192 × 96, echo time (TE): 3.95 ms, repetition time (TR): 11.25 ms]. Functional echo-planar imaging (EPI) scans were collected as 42 sagittal slices with an in-plane resolution of 1.5 × 1.5 mm and a slice thickness of 1.5 mm. The TR was 2.2 s, and the TE was 16 ms (FOV: 96 × 54 mm, matrix size: 64 × 36 mm, flip angle: 75°). Eye position was recorded using an MR-compatible infrared camera (MRC Systems, Heidelberg, Germany) fed into MATLAB (MathWorks, version R2018b) via a DATApixx hub (VPixx Technologies, Vision Science Solutions). We also acquired high-resolution T1-weighted whole-brain anatomical scans under sedation in a 4.7 T Bruker scanner with an MDEFT sequence. Imaging parameters were as follows: voxel size: 0.5 × 0.5 × 0.5 mm, TE: 4.9 ms, TR: 13.6 ms and flip angle: 14°. These scans were used to create a high-resolution template for each subject.

fMRI preprocessing

All EPI data were analyzed using Analysis of Functional NeuroImages (AFNI) software (http://afni.nimh.nih.gov/afni; Cox, 1996). Raw images were first converted from Bruker into AFNI data file format. The data collected in a single session were corrected for static magnetic field inhomogeneities using the PLACE algorithm (Xiang and Ye, 2007). The time-series data were then slice-time corrected and realigned to the last volume of the last run. All the data for a given subject were registered to the corresponding high-resolution template for that subject, allowing for the combination of data across multiple sessions. The first two volumes of data in each EPI sequence were disregarded. The volume registered data were then despiked and spatially smoothed with a 3 mm Gaussian kernel and rescaled to reflect percentage signal change from baseline.

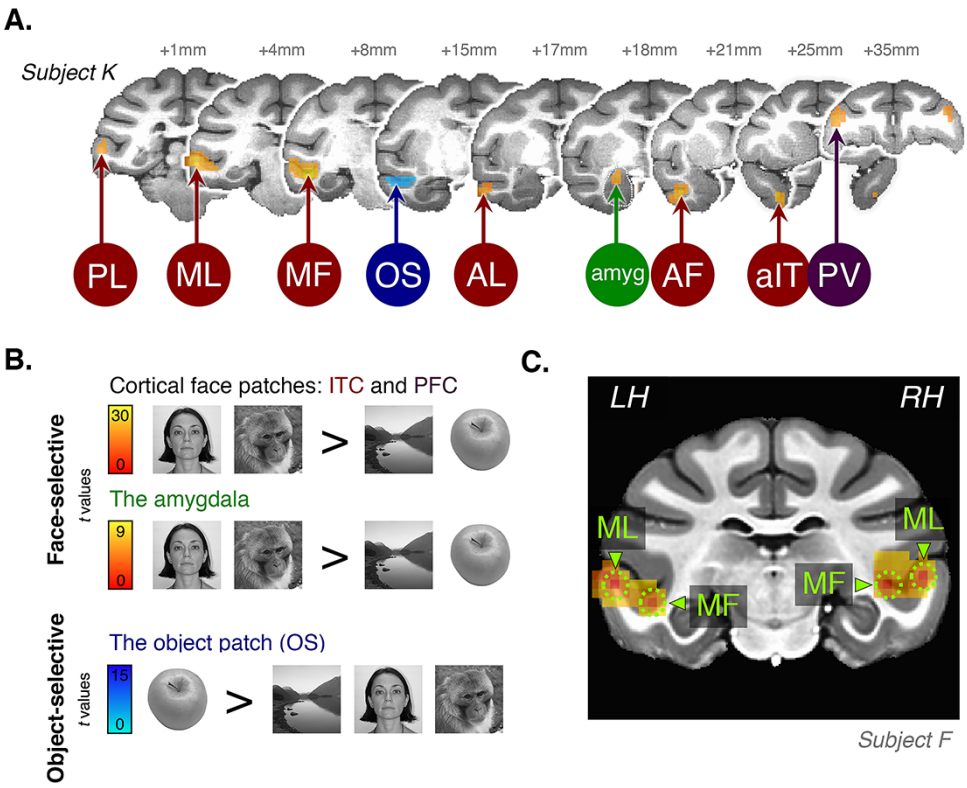

Fig. 1. Functional localization for Experiments 1 and 2. (A) Individual subject anatomy (*Subject K*) showing *t*-score maps for the face-selective (hot colors) and OS (blue colors) contrasts. The white dotted line approximates the anatomical boundary of the amygdala which was used to mask the localization data when defining the amygdala region of interest. (B) The contrasts used to define the ROIs in (A). (C) Localizer data from a single subject—this coronal slice (~6 mm anterior to the interaural line) illustrates the procedure localization of the separate face patches. Arrows point towards the location of the peak activations associated with the neighboring face patches, ML and MF. The dotted circular apertures represent the relative size of the spheres used to define the face patches.

Functional localizer

The functional localizer we used in this study has been described in detail elsewhere (see Taubert *et al.*, 2020a). For all six subjects, the face-selective patches were localized using the following contrast: (human faces + macaque faces) > (objects + scenes). This contrast revealed peak activations in the ITC corresponding to the face patches known as the posterior lateral face patch (PL), the middle lateral face patch (ML), the anterior lateral face patch (AL), the middle fundus face patch (MF) and the anterior fundus face patch (AF) (see Figure 1A). For most subjects, this contrast also isolated a sixth anterior face-selective region on the ventral surface of the brain; however, its exact anatomical location relative to the anterior middle temporal sulcus (*amts*) varied across subjects. Since we cannot know whether this region was the Anterior Medial face patch (AM; Tsao *et al.*, 2006) or the more recently identified face patches, thought to be involved in distinguishing familiar faces (see Landi and Freiwald, 2017), we have labeled this region the anterior ITC patch (aIT). All face patches were easily identifiable bilaterally in four subjects. In two subjects (F and J; Experiment 1), a separate peak activation corresponding to PL could not be identified, nor could aIT. The same procedure was used to identify the peak activation in the PV in each subject (Figure 1A). For Subject J, PV could only be identified in the left hemisphere.

We also defined the face-responsive regions of the amygdala because the amygdala has been theoretically linked to face detection behavior (Johnson, 2005) and casually linked to the perception of face pareidolia (Taubert *et al.*, 2018a). We note that face-selective neurons have been recorded in other subcortical structures (Nguyen *et al.*, 2013, 2016), but these structures could not be detected with the functional localizer used in this study. To define the amygdala region-of-interest, we first masked the localizer data using the anatomical boundary of the amygdala and then used the same contrast with the statistical threshold set at $P < 0.01$ (uncorrected). We used a different contrast to localize the OS patch in the STS: (objects) > (human faces + macaque faces + scenes) (see Figure 1B). This patch was always positioned between the middle STS face patches (ML and MF) and the anterior face patches (AL and AF; Figure 1A).

For the cortical ROIs, we drew spheres with a 2 mm radius around the peak activations in the localizer (Taubert *et al.*, 2020a). A 2 mm radius was necessary because it effectively separated the lateral edge patches from neighboring fundus patches (Figure 1C). This has proven to be an effective method of isolating separate face patches that is not dependent on setting an arbitrary statistical threshold (Taubert *et al.*, 2020a; for analysis of the ROIs, see Figure S1).

Because the face stimuli did not elicit a stronger response from early visual cortex (EVC) than the non-face stimuli, for the subjects in Experiment 1 we defined a proportion of EVC using the following contrast: (scrambled human faces + scrambled macaque faces) > implicit baseline. We employed a high statistical threshold ($P = 1 \times 10^{-15}$) to limit the voxels to foveal V1, V2 and V3, but for some subjects, this mask also included regions of V4 (see Figure S2). We note, however, that because the exact position of the headpost varied across subjects and was optimized for coverage

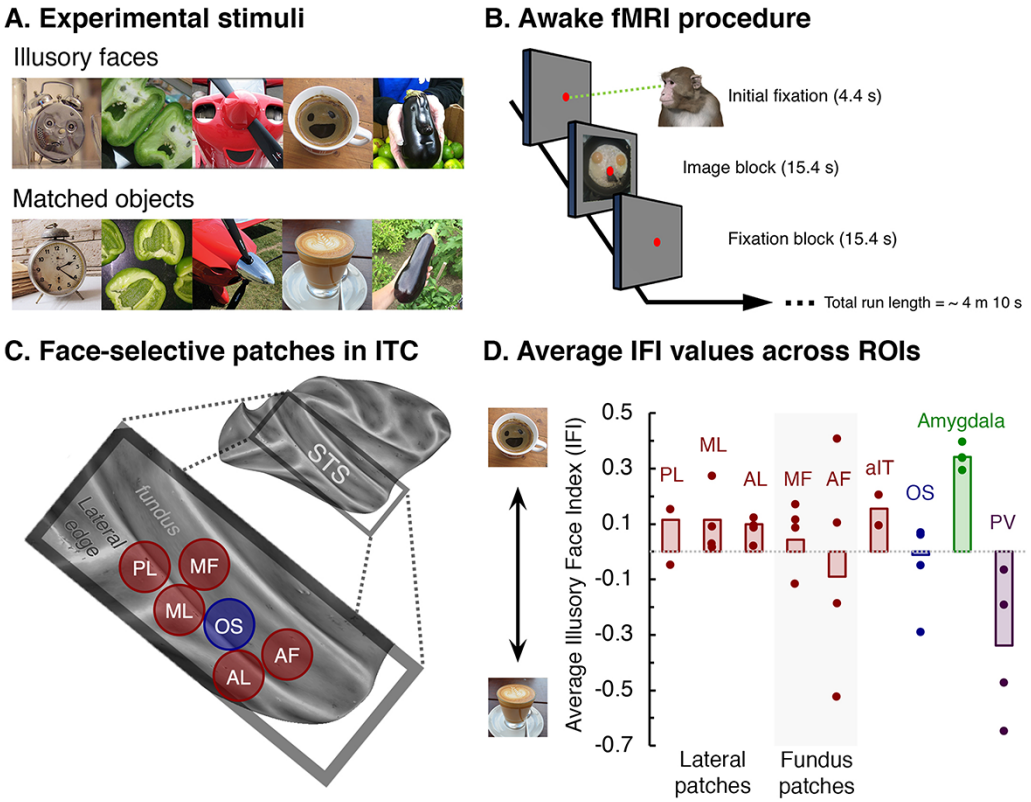

Fig. 2. A subset of face-selective regions responds more to illusory faces than objects (Experiment 1). (A) Example stimuli from both conditions in Experiment 1. (B) Schematic of the procedure for awake fMRI experiments. While in the scanner, subjects were awake and fixating on a small fixation spot. In Experiment 1, each run began with a 4.4 s fixation period followed by 16 blocks (8 stimulation and 8 fixation blocks presented in an alternating fashion). Each block was 15.4 s long. (C) Schematic indicating the relative position of the macaque face-selective and OS patches along the STS (side view of a right hemisphere; also see Figures S1 and S2 for more details). (D) Bar graph: the median *IFI* values as a function of ROI. Dots represent individual subject medians (for results of individual subject analyses, see Table S1).

of the temporal cortex, signal drop-out influenced the exact EVC regions that were sampled.

Experiment 1

Stimuli

A set of 56 color images of illusory faces were collected from the public domain using Google Image search (all images licensed for non-commercial reuse with modification). For each illusory face image, we also sourced a photograph of a similar object without an illusory face that matched the illusory face image as closely as possible (Figure 2A). Images were cropped to the same size (10° × 10° of visual angle). The 112 photographs were grouped into 8 unique image sets of 14 images each, with 4 illusory face sets and 4 matched object sets.

Experimental design and procedure

Experiment 1 used a high-powered on/off block design. Every run began with two dummy pulses and then 4.4 s of fixation before the onset of the experimental blocks. A small red fixation spot (0.5° diameter) remained on the screen for the entire duration of a run. The subjects were tasked with fixating on the red spot (within a fixation window that was 3° of visual angle in diameter). This fixation window was increased for Subject J to 4° in diameter. As long as the subjects maintained their fixation within the window, they received a juice reward approximately once every 2.2 s (±500 ms).

The 14 stimuli in each stimulus block were presented one at a time at the center of a gray screen, behind the fixation spot. The order of the stimuli in any given run was determined at random. Stimulus presentation was 900 ms with an ISI of 200 ms. Thus, all stimulation blocks were 15.4 s in duration, and each was followed by a 15.4 s fixation period (see Figure 2B). The order of the stimulation blocks was also determined at random. Each run lasted 250.8 s, during which we collected 114 volumes of data.

During the scan sessions, eye position was sampled and saved at 100 Hz. Subjects had to fixate within the fixation window for at least 60% of the run time for the data to be included in the analysis. Subject K completed 10 runs above this behavioral criterion (mean fixation = 76.5%). Subject F completed five runs (mean fixation = 85.8%). Subject S completed nine runs (mean fixation = 68.33%). Subject J only completed three runs above the behavioral criterion (mean fixation = 70%). To ensure that the results did not reflect an asymmetry in viewing behavior, for each subject we compared the number of valid eye position samples (i.e. the number of times the subject's eye position was within the fixation window) across the two conditions (i.e. illusory faces and matched objects) using a related-samples Wilcoxon signed rank test. We used 'run' as the unit of analysis. In doing so, we found no evidence that the subjects behaved differently toward illusory faces than they did toward matched objects (Subject K, $N = 10$, $P = 0.169$; Subject F, $N = 5$, $P = 0.893$; Subject S, $N = 9$, $P = 0.066$; Subject J, $N = 3$, $P = 1$).

Experiment 2

Stimuli

We used the 96 stimuli in Experiment 2 (32 human faces, 32 illusory faces and 32 matched objects). We used human faces rather than macaque faces to compare with illusory faces because these two face categories are better matched in terms of social relevance. Conspecific faces, even when unfamiliar to a subject, signal socially relevant cues such as dominance and social status, which are known to impact macaque behavior (Deaner *et al.*, 2005; Taubert *et al.*, 2019).

The three stimulus categories (human faces, illusory faces and matched objects) were further divided into two separate sets of images (herein referred to as Set 1 and Set 2) with 16 images in each set. Although this division was arbitrary for the human faces and the illusory faces, the objects remained matched with the corresponding illusory faces (e.g. if a green pepper with a face was allocated to 'Set 1', then the matched green pepper with no facial features was also allocated to 'Set 1').

Experimental design and procedure

Experiment 2 was similar to Experiment 1 except for the following details. There were 16 images per block, rather than 14, increasing the length of each block to 17.6 s. There were only 6 stimulation blocks (and 6 fixation blocks of equal length); thus, each run was 215.6 s in length during which we collected 98 volumes of data. Subjects had to fixate within the fixation window for at least 70% of the total length of a run for the data to be included in the subsequent analysis. Subject H completed 44 runs above this behavioral criterion (mean fixation = 83.43%), and Subject A completed 46 runs (mean fixation = 86%). Again, to ensure that the results did not reflect an asymmetry in viewing behavior, for each subject we compared the number of valid eye position samples across the three conditions using a Freidman test. We found no evidence that subject behavior differed across conditions (Subject H, $N = 44$, $P = 0.913$; Subject A, $N = 46$, $P = 0.913$).

Data analysis

General linear model

For the data collected in Experiment 1, we convolved the hemodynamic response function following MION exposure (inverted for positive beta values) with the two regressors of interest (illusory faces and matched objects) using an ordinary least squares regression (executed using the AFNI function '3dDeconvolve'). The regressors of no interest included in the model were six motion regressors and three baseline estimates per run (i.e. constant, linear and quadratic). Thus, each voxel had two beta coefficients corresponding to the two regressors of interest. Statistical comparisons between face-selective voxel and OS voxel were performed using custom scripts written in MATLAB (MathWorks, version R2018b). We used the same procedure for Experiment 2, except there were three regressors of interest (illusory faces, matched objects and human faces) rather than two.

Category cross-decoding and representational similarity analysis

For the cross-decoding procedure, we computed beta coefficients for each of the six unique stimulus blocks on a run-by-run basis. To achieve this, we convolved the hemodynamic response function with six regressors of interest (illusory faces Set 1, illusory faces Set 2, matched objects Set 1, matched objects Set 1, human faces Set 1 and human faces Set 2) using the AFNI function '3dDeconvolve' with the individual modulation flag. Thus, each voxel had six beta coefficients computed for each run included in the model (for Subject H, $n = 44$, and for Subject A, $n = 46$). The decoding analyses were performed separately for each subject in their native brain space in MATLAB using functions from the Decoding Toolbox (Hebart *et al.*, 2014). Classification was performed using a linear support vector machine. The classifier was trained on the data for a pair of stimulus sets (e.g. Set 1 illusory faces *vs* Set 2 matched objects) with the data from one run held out. Next, the classifier was tested on the held-out data for a pair of stimulus sets (e.g., Set 2 illusory faces *vs* Set 2 matched objects). Then, classification was repeated with the test and training sets swapped. This entire procedure was then repeated so that each run was left out once. The advantage of this method is that above chance decoding performance indicates that the classifier was able to discriminate the face condition from the non-face condition after generalizing to independent stimuli not used in the training set and based on independent data. Therefore, successful decoding cannot reflect the neural response to low-level visual features associated with particular stimuli.

Results (Experiment 1)

To explore the response of the cortical face patches (Figure 2C) and other face-selective regions, to illusory faces we measured brain activity during an fMRI experiment. For every voxel in the ROIs, we computed an Illusory Face Index $[IFI = (\beta_{\text{illusory faces}} - \beta_{\text{objects}})/(|\beta_{\text{illusory faces}}| + |\beta_{\text{objects}}|)]$ (Taubert *et al.*, 2020b). Thus, *IFI* values greater than zero indicate that the voxel responded, on average, more to the objects with illusory facial features than the matched non-face objects. For each ROI, we used a one-sample Wilcoxon signed rank test (two-tailed) to determine whether the median *IFI* value across voxels was greater than zero (Figure 2D). This was the case for the PL ($N = 34$, *Median* = 0.11, $P < 0.001$), ML ($N = 68$, *Median* = 0.12, $P < 0.001$) and AL ($N = 64$, *Median* = 0.10, $P < 0.001$) face patches, as well as the amygdala ($N = 405$, *Median* = 0.34, $P < 0.001$). We also found evidence that voxels in the neighboring OS patch in the ITC ($N = 60$, *Median* = −0.01, $P = 0.025$), together with those in the PV face patch ($N = 61$, *Median* = −0.34, $P < 0.001$), responded consistently more to matched objects with no facial features than to objects with facial features. However, we found no evidence that the voxels in MF ($N = 72$, *Median* = 0.04, $P = 0.079$), AF ($N = 66$, *Median* = −0.09, $P = 0.106$) or aIT ($N = 28$, *Median* = 0.15, $P = 0.111$) responded differentially to objects with or without facial features.

To determine whether our results above reflected a general bias toward face-like stimuli within the visual system, we also tested a functionally defined section of EVC. For these voxels, we computed the *IFI* and then tested whether the median value was greater than zero. In contrast to when we tested some of the face patches, we found that EVC responded more to the matched objects than illusory faces ($N = 9232$, *Median* = −0.06, $P < 0.0001$). Individual subject data are reported in Figure S2. Therefore, if anything, the earlier stages of visual processing responded more to the matched objects than the illusory faces.

Overall, we found the lateral face patches (specifically PL, ML and AL) were more sensitive to examples of face pareidolia than their counterparts in the fundus of the STS (MF and AF; Figure 1D). The amygdala was the only other region exhibiting a reliably greater response to illusory faces than matched objects although the aIT face patch had a high *IFI* median value (Figure 1D).

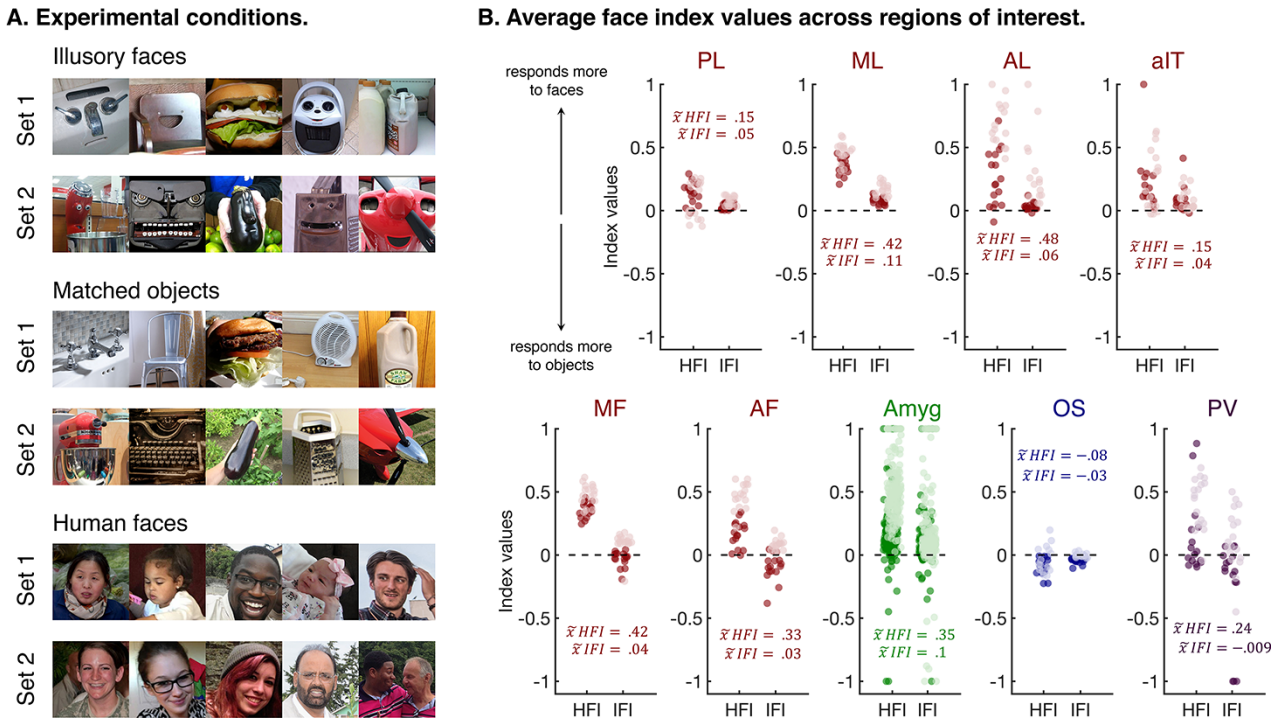

Fig. 3. Voxel-wise response to human and illusory faces in the ROIs (Experiment 2). (A) Examples of stimuli from the six stimulus blocks in Experiment 2. (B) Plots show the HFI and the IFI for individual voxels in each region of interest (*Subject H* = light colors, *Subject A* = dark colors). Note that HFI and IFI values are plotted separately for each voxel, so that each voxel is represented twice in each subplot. Values are plotted with some jitter (*x*-axis only) for improved visualization.

Results (Experiment 2)

In Experiment 2, we measured the response of the ROIs to real faces, illusory faces and matched objects (Figure 3A). We calculated a *human face index* [$HFI = (\beta_{\text{human faces}} - \beta_{\text{objects}})/(|\beta_{\text{human faces}}| + |\beta_{\text{objects}}|)$] and an *IFI* for all voxels in the ROIs. We analyzed each subject's data, separately, using a mixed design 2 × 9 analysis of variance with *Index* as the repeated factor and *Region* as the group factor (the Greenhouse–Geisser correction was used for violations of sphericity). For *Subject H*, we found a main effect of *Index* ($F[1277] = 149.28$, $P < 0.001$, $\eta_p^2 = 0.35$), indicating that *HFI* values ($M = 0.37$, $SEM = 0.02$) were higher than *IFI* values ($M = 0.12$, $SEM = 0.02$). The main effect of *Region* ($F[8, 277] = 10.54$, $P < 0.001$, $\eta_p^2 = 0.23$) also indicated that index values differed across the ROIs. Of particular interest was the significant interaction effect between *Index* and *Region* ($F[8, 277] = 7.53$, $P < 0.001$, $\eta_p^2 = 0.18$; Figure 3B). To find the source of this variation, we ran nine pairwise comparisons testing the difference between *HFI* and *IFI* values for each region of interest. We found that *HFI* values were greater than *IFI* values in the amygdala (*Mean Diff* = 0.33, *SEM* = 0.02, $P < 0.001$) and all face-selective patches (ML, *Mean Diff* = 0.3, *SEM* = 0.06, $P < 0.001$; AL, *Mean Diff* = 0.38, *SEM* = 0.07, $P < 0.001$; MF, *Mean Diff* = 0.38, *SEM* = 0.06, $P < 0.001$; AF, *Mean Diff* = 0.38, *SEM* = 0.06, $P < 0.001$; aIT, *Mean Diff* = 0.15, *SEM* = 0.06, $P = 0.016$; PV, *Mean Diff* = 0.28, *SEM* = 0.06, $P < 0.001$) except PL (*Mean Diff* = 0.005, *SEM* = 0.06, $P = 0.942$). As predicted, no such difference between *HFI* and *IFI* values was present in the OS patch (*Mean Diff* = –0.03, *SEM* = 0.06, $P = 0.634$; Figure 3B).

The analysis of *Subject A*'s data revealed the same pattern of results as *Subject H* (*Index*, $F[1, 241] = 78.85$, $P < 0.001$, $\eta_p^2 = 0.25$; *Region*, $F[8, 241] = 6.85$, $P < 0.001$, $\eta_p^2 = 0.18$; *Index*Region*, $F[8, 241] = 5.74$, $P < 0.001$, $\eta_p^2 = 0.16$; Figure 3B). Again, *HFI* values ($M = 0.18$, $SEM = 0.02$) were, on average, higher than *IFI* values ($M = -0.01$, $SEM = 0.01$). When unpacking the significant interaction between *Index* and *Region*, we found that *HFI* values were higher than *IFI* values in the amygdala (*Mean Diff* = 0.07, *SEM* = 0.03, $P = 0.007$) and all face-selective patches (ML, *Mean Diff* = 0.27, *SEM* = 0.07, $P < 0.001$; AL, *Mean Diff* = 0.22, *SEM* = 0.07, $P = 0.001$; MF, *Mean Diff* = 0.39, *SEM* = 0.07, $P < 0.001$; AF, *Mean Diff* = 0.26, *SEM* = 0.07, $P < 0.001$; PV, *Mean Diff* = 0.38, *SEM* = 0.07, $P < 0.001$) except PL (*Mean Diff* = 0.11, *SEM* = 0.07, $P = 0.12$) and aIT (*Mean Diff* = 0.14, *SEM* = 0.08, $P = 0.057$). Again, there was no difference between *HFI* and *IFI* values in the OS patch (*Mean Diff* = 0.05, *SEM* = 0.07, $P = 0.514$; Figure 3B). In sum, in both subjects, we found that the majority of cortical face patches (excluding PL in both subjects and aIT in one subject) and the amygdala responded more selectively to photographs of human faces than to photographs of face pareidolia.

Sensitivity to illusory faces among the ROIs

We combined the *IFI* values from both subjects and computed grand median *IFI* values for each region of interest. To test whether each region responded more to illusory faces than matched objects, we used one-sample Wilcoxon signed rank tests (two-sided). In doing so, we found strong evidence that the lateral face patches in STS were all sensitive to illusory facial features in ordinary objects (PL, $N = 33$, *Median* = 0.05, $P < 0.001$; ML, $N = 32$, *Median* = 0.11, $P < 0.001$; AL, $N = 32$, *Median* = 0.06, $P < 0.001$). While we found that the aIT face patch, positioned on the ventral surface of the brain, was also sensitive to illusory facial features ($N = 31$, *Median* = 0.04, $P < 0.001$), not all of the face patches in the ITC shared this sensitivity. In fact, there was no evidence that either of the face patches seated in the fundus of the STS were sensitive to illusory facial features

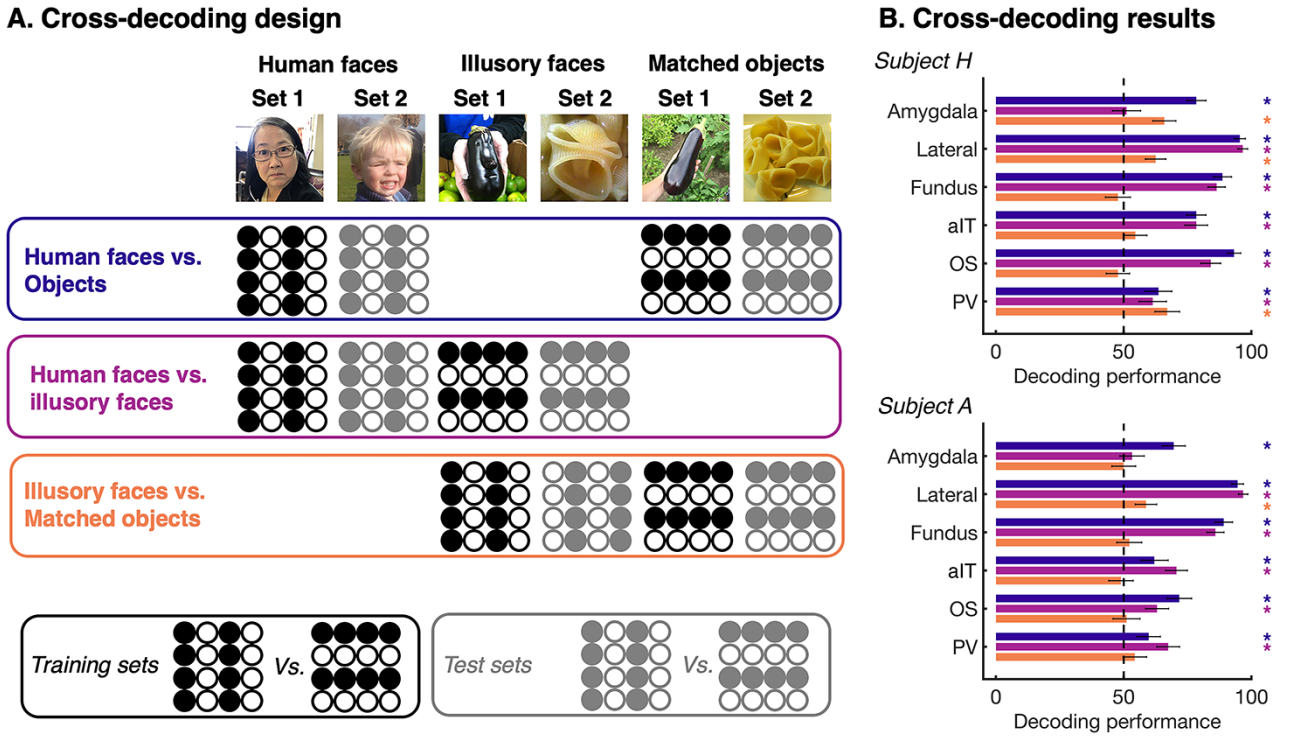

Fig. 4. Human faces and illusory faces produce distinct activation patterns in the lateral face patches but not in the amygdala (Experiment 2). (A) Schematic of the design for three types of category cross-decoding: human faces *vs* objects, human faces *vs* illusory faces and illusory faces *vs* objects. Circles indicate example stimulus sets used for training (black) *vs* testing (gray) the classifier in each case. Note that the classifier is trained and tested on data from different stimuli (image sets) within each category (i.e. cross decoding). (B) Classifier performance for Subject H and Subject A (bottom) as a function of region (i.e. amygdala, lateral face patches, fundus face patches, aIT, OS and PV). Bar colors reflect the type of cross decoding (blue = human faces *vs* objects; pink = human faces *vs* illusory faces; orange = illusory faces *vs* matched objects). The dashed line indicates numerical chance (50%). An asterisk indicates performance is above chance (one-sample *t*-test, $P < 0.05$, see Table 1 for the results associated with the discrete face patches).

(MF, $N = 32$, *Median* = 0.04, $P = 0.07$; AF, $N = 32$, *Median* = 0.03, $P = 0.93$).

Interestingly, when we tested the other ROIs, we found that the OS patch responded more to objects without facial features than illusory faces ($N = 31$, *Median* = –0.03, $P < 0.001$). This result indicates the voxel suppresses its response to objects in the presence of illusory facial features (also see Figure S4). As in Experiment 1, the amygdala responded more to illusory faces then objects ($N = 279$, *Median* = 0.10, $P < 0.001$). However, we found no evidence that the PV face patch was sensitive to illusory facial features ($N = 34$, *Median* = –0.009, $P = 0.92$).

Cross-decoding reveals a difference between cortical and subcortical mechanisms

We used a category cross-decoding approach as the critical test for defining whether different brain regions were sensitive to the presence or absence of illusory facial features. The leave-one-run-out cross-decoding procedure is described in detail in the 'Method' section (also see Figure 4A). We combined the data from the lateral face patches and the fundus patches because these regions are thought to be anatomically and functionally distinct (Tsao and Livingstone, 2008; Freiwald and Tsao, 2010; Freiwald *et al.*, 2016; Taubert *et al.*, 2020a; Pitcher and Ungerleider, 2021). Thus, for the purposes of this analysis there are six ROIs: (i) the amygdala, (ii) the lateral face patches (PL, ML and AL combined), (iii) the fundus face patches (MF and AF combined), (iv) the aIT face patch, (v) the OS patch and (vi) the PV face patch. For both subjects, human faces could be successfully decoded from objects from the patterns of brain activation in all regions (Figure 4B, *blue bars*). These results confirm that the face-selective region and the OS region identified using the independent localizer respond differently to photographs of unfamiliar human faces than they do to photographs of ordinary objects.

Consistent with the results of the univariate analyses in both Experiments 1 and 2, illusory faces were decodable from matched objects in the lateral edge face patches but not the fundus face patches (Figure 4B, *orange bars*). These results further indicate that, unlike the fundus face patches, the lateral face patches respond more to illusory faces than matched objects. We could not decode illusory faces from matched objects based on the patterns of activation in AM. For the amygdala, we found that illusory faces were decodable from matched objects in one subject but not the other. The same subject differences occurred for the PV patch. Although we caution against overinterpreting these results, we note that both the amygdala and the ventral lateral prefrontal cortex are multimodal regions known to respond broadly to lots of different visual stimuli (Mormann *et al.*, 2011; Romanski and Diehl, 2011; Cleeren *et al.*, 2020; Visser *et al.*, 2021). It is likely, therefore, that some of our non-face images (both illusory faces and matched objects) would have evoked strong responses from these regions making the 'illusion faces *vs* matched objects' decoding task more difficult. All results are available in Table 1.

Table 1. Classifier performance (% correct)

Patch	Subject	Type	Mean	SEM	P-value	Sig.
PL	H	HF *vs* MO	81.81818	3.667939	<0.001	*
		HF *vs* IF	75	4.451999	<0.001	*
		IF *vs* MO	56.8182	5.53456	0.23	NS
	A	HF *vs* MO	80.43478	3.955752	<0.001	*
		HF *vs* IF	82.6087	3.549985	< 0.001	*
		IF *vs* MO	42.3913	5.376499	0.164	NS
ML	H	HF *vs* MO	90.9091	3.36029	<0.001	*
		HF *vs* IF	84.0909	4.23064	<0.001	*
		IF *vs* MO	59.0909	4.07148	0.031	*
	A	HF *vs* MO	94.5652	2.31997	<0.001	*
		HF *vs* IF	91.3043	2.82516	< 0.001	*
		IF *vs* MO	60.8696	5.1342	0.04	*
AL	H	HF *vs* MO	90.90909	2.940894	<0.001	*
		HF *vs* IF	90.90909	2.940894	<0.001	*
		IF *vs* MO	55.68182	5.195926	0.28	NS
	A	HF *vs* MO	93.47826	2.952398	<0.001	*
		HF *vs* IF	92.3913	2.67724	<0.001	*
		IF *vs* MO	58.69565	4.478706	0.058	NS
MF	H	HF *vs* MO	88.63636	3.19538	<0.001	*
		HF *vs* IF	86.36364	3.395852	<0.001	*
		IF *vs* MO	54.54545	3.921192	0.253	NS
	A	HF *vs* MO	90.21739	2.956841	<0.001	*
		HF *vs* IF	83.69565	3.494076	<0.001	*
		IF *vs* MO	53.26087	4.505009	0.473	NS
AF	H	HF *vs* MO	90.90909	3.360292	<0.001	*
		HF *vs* IF	88.63636	3.19538	<0.001	*
		IF *vs* MO	43.18182	4.764793	0.16	NS
	A	HF *vs* MO	89.13043	3.074377	<0.001	*
		HF *vs* IF	83.69565	3.824138	<0.001	*
		IF *vs* MO	50	4.662524	>0.9	NS
aIT	H	HF *vs* MO	78.40909	3.776851	<0.001	*
		HF *vs* IF	78.40909	4.42154	<0.001	*
		IF *vs* MO	47.72727	4.86459	0.643	NS
	A	HF *vs* MO	61.95652	5.425112	<0.001	*
		HF *vs* IF	70.65217	4.277818	0.033	*
		IF *vs* MO	48.91304	4.787547	0.821	NS

P-values computed using a one-sample t-test (two-tailed; chance = 50%).
An asterisk (*) indicates performance is above chance (i.e. $P < 0.05$, uncorrected). Bold text indicates regions where all pairwise comparisons are significant.

Surprisingly, while decoding between human faces and illusory faces was significant in *all* cortical ROIs (including the fundus face patches), this was not the case for the face-selective amygdala region (Figure 4B, *pink bars*). This difference between the amygdala and the cortical face patches suggests that the regions of the amygdala that are sensitive to faces are also *insensitive* to the difference between human faces and illusory faces. If illusory faces are represented more similarly to human faces in the amygdala than they are in the lateral face patches, they would elicit more similar activation patterns, which in turn would make classification more difficult. We explore this idea next using representational similarity analysis.

Human and illusory faces are represented similarly in the amygdala

To compare the representation of illusory faces in the lateral face patches to the representation of illusory faces in the amygdala, we applied representational similarity analysis (Kriegeskorte *et al.*, 2008; Wardle *et al.*, 2020). Given that illusory faces on objects have a dual identity (face + object), we were interested in whether illusory faces were represented more similarly to objects or to human faces in these regions which responded to face pareidolia (Figure 5A). Accordingly, we calculated separate representational dissimilarity matrices (RDMs) for the amygdala and the lateral face patches. Unlike the data for the decoding analysis, the RDMs were calculated by correlating beta values (averaged across runs) for each pair of stimulus categories [human faces (HF), illusory faces (IF) and matched objects (MO)]. Then, we computed *1-correlation* to produce a dissimilarity score. Therefore, the source of any differences evident between the cross-decoding results and other results, including the RSA, is likely to be variation across runs and/or variation in the response to the discrete image sets.

Interestingly, the RDMs for the lateral face patches suggest that illusory faces are represented more similarly to objects than to human faces (Figure 5B). On the other hand, in the amygdala illusory faces produced activation patterns more similar to those for human faces. This difference supports the results of the cross-decoding analysis by showing that the amygdala builds a representation of faces that is distinct from that in the ITC. For comparison, we also included the fundus face patches and the OS patch in the analysis. Overall, these observations imply that the similarity between illusory faces and matched objects dominates the representation of illusory objects in the ITC. This is consistent with the reality that examples of face pareidolia are inanimate objects and not social agents. There is also evidence from the human brain that the cortical visual system quickly resolves the

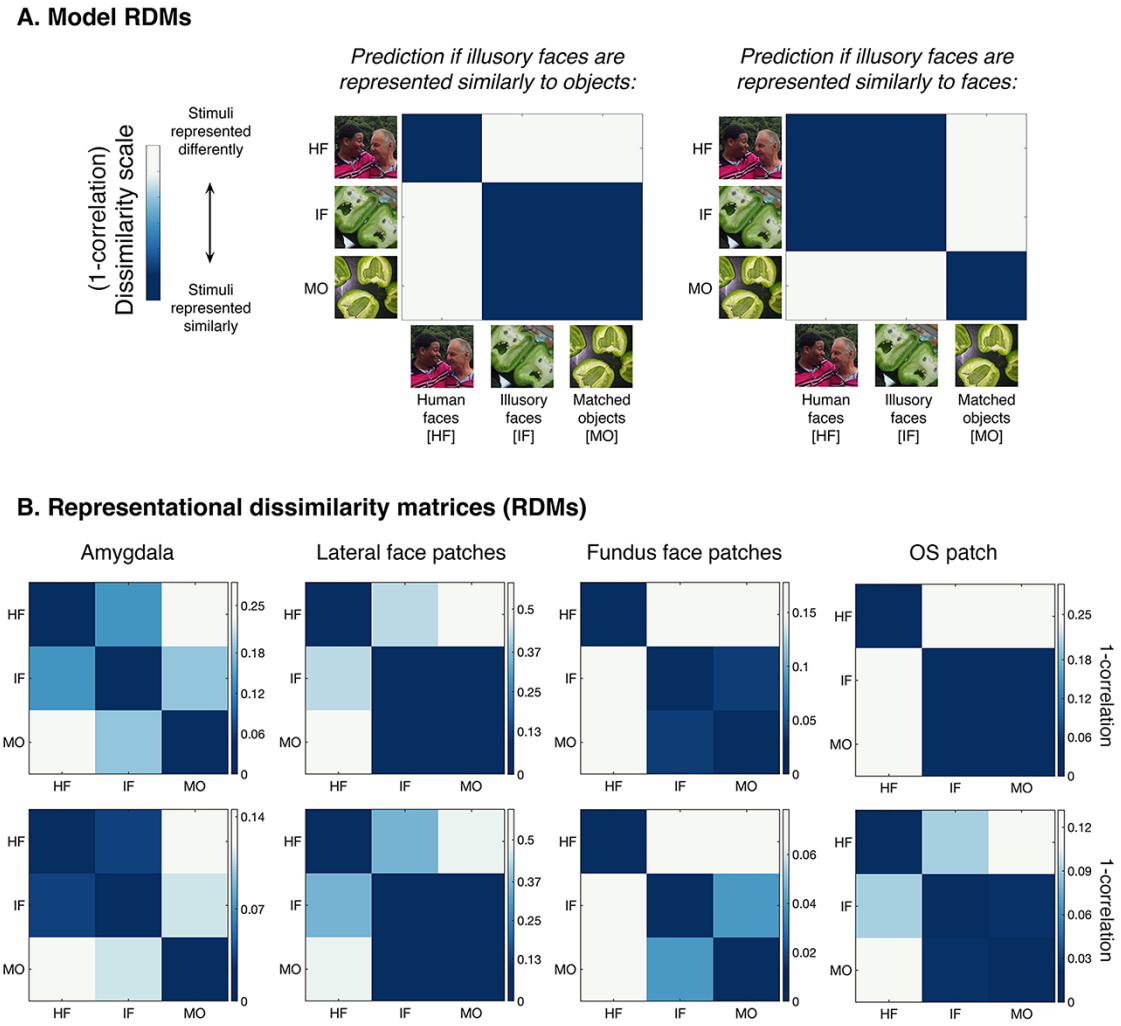

Fig. 5. RSA reveals distinct representations of illusory faces in the amygdala and lateral face patches. (A) Model RDMs based on the expected results if illusory faces are represented more similarly to objects or (bottom) more similarly to faces. (B) Empirical RDMs for the amygdala and the lateral face patches for Subject H (*top row*) and Subject A (*bottom row*). Corresponding RDMs were also generated for the fundus face patches and the OS patch. RDMs show the pairwise dissimilarity (1—correlation) in activation patterns evoked by each stimulus category (HF, IF and MO).

erroneous detection of a face and ultimately represents examples of face pareidolia as objects, not faces (Wardle *et al.*, 2020).

Discussion

In this study, we demonstrate in six rhesus macaques that a particular class of objects recruits a number of brain regions thought to be specialized for processing faces (Figures 2D and 3B). This class of objects is highly heterogeneous, comprised of exemplars that only have one thing in common; they each coincidently possess illusory facial features (face pareidolia). Because naturally occurring examples of face pareidolia have been shown to elicit the behavioral markers of face detection and prioritization in humans and macaques (Taubert *et al.*, 2017; Omer *et al.*, 2019; Wardle *et al.*, 2020; Caruana and Seymour, 2022; Keys *et al.*, 2021; Wardle *et al.*, 2022), the select involvement of the lateral face patches in the ITC and the amygdala demonstrates that the detection of face stimuli during natural viewing is governed by a multiplexed system comprised of both cortical and subcortical regions (Johnson, 2005).

In both experiments, we discovered that the face patches on the lower lateral edge of the STS, namely, PL, ML and AL, were driven by the illusion of facial features in common examples of face pareidolia (Figures 2D and 3B). The finding that the PL and ML face patches responded more to illusory faces than matched objects (Figures 2D and 3B) is consistent with a role in face detection, as has been previously suggested by studies of activity at the level of the single neuron (Freiwald and Tsao, 2010; Issa and DiCarlo, 2012; Ohayon *et al.*, 2012; Taubert *et al.*, 2015a). Recently, an inactivation study confirmed that silencing activity in ML attenuated detection performance in a visual search task by ∼11% when the target was a face (Sadagopan *et al.*, 2017). Importantly, inactivating ML did not reduce face detection performance to chance, indicating that other mechanisms also support the behavior. Nonetheless, when combined with the current results, there is now a confluence of evidence to suggest that ML, together with PL and AL, plays a role in the detection of face-like forms (Tsao and Livingstone, 2008).

Furthermore, by demonstrating that the lateral face patches are sensitive to examples of face pareidolia, these data also provide evidence that PL, ML and AL may be functional homologs of the human occipital face area (OFA) and fusiform face area (FFA) (Yovel and Freiwald, 2013; Wardle *et al.*, 2020). This homology has been contentious, particularly because of the absence of

the fusiform gyrus in the macaque brain which is considered an important anatomic landmark for face processing in the human brain (see Rossion and Taubert, 2019). However, a recent human imaging study using the exact same stimulus set as we used in Experiment 2 found that OFA and FFA respond more to illusory faces than matched objects, unlike the corresponding object- and scene-selective areas in the human brain (Wardle *et al.*, 2020). This was also confirmed with a category cross-decoding procedure (Wardle *et al.*, 2020), similar to what was used here (Figure 4B). Taken together with the current results, it seems likely that the human OFA and FFA play similar roles in face detection as the macaque lateral face patches.

Although the lateral face patches were engaged by illusory faces, we found that the fundus face patches (AF and MF) were not (Figures 3B and 4B). Prior to the current study, the only experiments that have decoupled the lateral face patches from the fundus face patches with static images have manipulated facial expressions and movement (Furl *et al.*, 2012; Taubert *et al.*, 2020a). A prominent theory posits that the fundus face patches are part of a separate processing pathway that promotes social cognition (Pitcher and Ungerleider, 2021). Thus, we would argue that a possible explanation for the response of the fundus face patches to illusory faces is that they were not recognized as social agents. Even so, this finding is important in demonstrating a key functional difference between the lateral face patches and the neighboring fundus face patches. A related possibility is that the lack of motion in illusory faces is relevant to why they do not appear to engage the fundal face patches (Fisher and Freiwald, 2015).

We note that other additional face patches in the temporal (Landi and Freiwald, 2017; Landi *et al.*, 2021) and prefrontal (Tsao *et al.*, 2008) lobes have been recently identified in the literature, as well as discrete sub-populations of face-selective neurons (Park *et al.*, 2017). We were unable to locate these regions using our static localizer (for more details, see the 'Method' section and Taubert *et al.*, 2020a,b); thus, they were not analyzed as part of this study. Although these patches are thought to contribute more to the memory/learning aspects of face recognition (Landi and Freiwald, 2017), it remains possible that they also play an important role in face detection.

In the second experiment, we compared activity in response to real human faces and illusory faces. Both face-selective and OS patches in the ITC easily discriminated real human faces from illusory faces (Figure 4B). However, a surprise finding was that patterns of activity within the amygdala could not discriminate real faces from illusory faces (Figure 4B). Close inspection of the activation patterns suggested that illusory faces are encoded more similarly to human faces in the amygdala, whereas illusory faces are encoded more similarly to objects in the ITC (Figure 5B). This finding is consistent with a recent lesion study, showing that behavior toward both real and illusory faces was equally disrupted following amygdala loss (Taubert *et al.*, 2018a). This suggests that the amygdala builds representations of face stimuli based on different principles than the face patches in the ITC. That is, the amygdala may not be as tightly tuned to the specific visual properties that typically define real primate faces, such as skin/hair colors or a round outer contour. Instead, the amygdala might be part of a circuit that is sensitive to a rudimentary template used for detecting socially relevant visual stimuli in the environment and subsequently allocating attentional resources (de Gelder *et al.*, 2003; Johnson, 2005; Tamietto and de Gelder, 2010). Other studies have also linked other subcortical structures to a rudimentary form of face detection (Nguyen *et al.*, 2013, 2016; Omer *et al.*, 2019; Caruana and Seymour, 2022) that relies on a basic blueprint or 'face-like template' (Johnson, 2005). Although the current results cannot speak to the role of the pulvinar or superior colliculus in face detection, it highlights the importance of considering the role of subcortical structures in complex visual behaviors that are often assumed to have a cortical locus.

These findings, while consistent with an emerging literature (Taubert *et al.*, 2017, 2020b; Wardle *et al.*, 2020; Alais *et al.*, 2021; Decramer *et al.*, 2021; Keys *et al.*, 2021; Wardle *et al.* 2022), beg the question—what features do examples of face pareidolia share with real faces? In other words, what features drive the detection of a face? While previous work has not identified clear low- or mid-level visual properties that real and illusory faces share in common (Wardle *et al.*, 2020), it remains possible that the behavioral and neural signatures of face detection are driven by the presence of eyes (Issa and DiCarlo, 2012) or a specific contrast envelope (Ohayon *et al.*, 2012). More research is needed to distill the exact features that trigger the detection and perception of faces in natural scenes.

Here, using the correlates of illusory faces in the macaque brain, we provide evidence for two complementary cortical and subcortical mechanisms for face detection: the lateral face patches in the ITC and the amygdala. Based on these results, we propose that the amygdala might be coarsely tuned to visual features diagnostic of a face such that it responds to both illusory and real faces similarly, whereas the lateral face patches in the ITC might be more tightly tuned to the fine-grained image properties that distinguish real faces from both illusory faces and non-face objects. It remains unclear which of these representations, if any, are directly linked to perceptual awareness. A potential advantage of having a multiplexed system for face detection with different cortical and subcortical mechanisms tuned to different visual properties is that it likely produces increased sensitivity paired with the rapid resolution of face detection errors.

Acknowledgements

Functional and anatomical MRI scanning was carried out in the Neurophysiology Imaging Facility Core (the National Institute of Mental Health (NIMH), the National Institute of Neurological Disorders and Stroke, and the National Eye Institute) with special thanks to David Yu, Aidan P. Murphy, Charles Zhu and Frank Ye for technical assistance. We also thank Dr Christopher I. Baker of the NIMH for his helpful feedback.

Funding

This research was supported by the Intramural Research Program of the National Institute of Mental Health (ZIAMH002918 to L.G.U.) and the Australian Research Council (FT200100843 to J.T.).

Conflict of interest

The authors declared that they had no conflict of interest with respect to their authorship or the publication of this article.

Supplementary data

Supplementary data are available at *SCAN* online.

Author contributions

J.T., S.G.W. and L.G.U. designed the study and programmed the experimental tasks. C.T.T., E.A.K., S.K. and J.T. collected the data. J.T., S.K. and A.M. preprocessed the EPI data. J.T., S.G.W. and S.K.

analyzed the data. J.T. and S.G.W. wrote the original manuscript under the careful supervision of L.G.U. All authors assisted with editing the manuscript.

References

Alais, D., Xu, Y., Wardle, S.G., Taubert, J. (2021). A shared mechanism for facial expression in human faces and face pareidolia. *Proceedings of the Royal Society B: Biological Sciences*, **288**(1954), 20210966.

Bell, A.H., Malecek, N.J., Morin, E.L., Hadj-Bouziane, F., Tootell, R.B., Ungerleider, L.G. (2011). Relationship between functional magnetic resonance imaging-identified regions and neuronal category selectivity. *The Journal of Neuroscience: The Official Journal of the Society for Neuroscience*, **31**(34), 12229–40.

Caruana, N., Seymour, K. (2022). Objects that induce face pareidolia are prioritized by the visual system. *British Journal of Psychology*, **113**(2), 496–507.

Cleeren, E., Popivanov, I.D., Van Paesschen, W., Janssen, P. (2020). Fast responses to images of animate and inanimate objects in the nonhuman primate amygdala. *Scientific Reports*, **10**(1), 14956.

Cox, R.W. (1996). AFNI: software for analysis and visualization of functional magnetic resonance neuroimages. *Computers and Biomedical Research*, **29**(3), 162–73.

Crouzet, S.M., Kirchner, H., Thorpe, S.J. (2010). Fast saccades toward faces: face detection in just 100 ms. *Journal of Vision*, **10**(4), 16.11–17.

de Gelder, B., Frissen, I., Barton, J., Hadjikhani, N. (2003). A modulatory role for facial expressions in prosopagnosia. *Proceedings of the National Academy of Sciences of the United States of America*, **100**(22), 13105–10.

Deaner, R.O., Khera, A.V., Platt, M.L. (2005). Monkeys pay per view: adaptive valuation of social images by rhesus macaques. *Current Biology: CB*, **15**(6), 543–8.

Decramer, T., Premereur, E., Zhu, Q., *et al.* (2021). Single-unit recordings reveal the selectivity of a human face area. *The Journal of Neuroscience: The Official Journal of the Society for Neuroscience*, **41**(45), 9340–9.

Fenske, M.J., Eastwood, J.D. (2003). Modulation of focused attention by faces expressing emotion: evidence from flanker tasks. *Emotion (Washington, D.C.)*, **3**(4), 327–43.

Fisher, C., Freiwald, W.A. (2015). Contrasting specializations for facial motion within the macaque face-processing system. *Current Biology*, **25**(2), 261–6.

Freiwald, W., Duchaine, B., Yovel, G. (2016). Face processing systems: from neurons to real-world social perception. *Annual Review of Neuroscience*, **39**, 325–46.

Freiwald, W.A., Tsao, D.Y. (2010). Functional compartmentalization and viewpoint generalization within the macaque face-processing system. *Science*, **330**(6005), 845–51.

Furl, N., Hadj-Bouziane, F., Liu, N., Averbeck, B.B., Ungerleider, L.G. (2012). Dynamic and static facial expressions decoded from motion-sensitive areas in the macaque monkey. *The Journal of Neuroscience: The Official Journal of the Society for Neuroscience*, **32**(45), 15952–62.

Gamer, M., Schmitz, A.K., Tittgemeyer, M., Schilbach, L. (2013). The human amygdala drives reflexive orienting towards facial features. *Current Biology: CB*, **23**(20), R917–8.

Goren, C.C., Sarty, M., Wu, P.Y. (1975). Visual following and pattern discrimination of face-like stimuli by newborn infants. *Pediatrics*, **56**(4), 544–9.

Grimaldi, P., Saleem, K.S., Tsao, D. (2016). Anatomical connections of the functionally defined "face patches" in the macaque monkey. *Neuron*, **90**(6), 1325–42.

Hadj-Bouziane, F., Bell, A.H., Knusten, T.A., Ungerleider, L.G., Tootell, R.B. (2008). Perception of emotional expressions is independent of face selectivity in monkey inferior temporal cortex. *Proceedings of the National Academy of Sciences of the United States of America*, **105**(14), 5591–6.

Hebart, M.N., Görgen, K., Haynes, J.D. (2014). The Decoding Toolbox (TDT): a versatile software package for multivariate analyses of functional imaging data. *Frontiers in Neuroinformatics*, **8**, 88.

Issa, E.B., DiCarlo, J.J. (2012). Precedence of the eye region in neural processing of faces. *The Journal of Neuroscience: The Official Journal of the Society for Neuroscience*, **32**(47), 16666–82.

Johnson, M.H. (2005). Subcortical face processing. *Nature Reviews Neuroscience*, **6**(10), 766–74.

Kanwisher, N., McDermott, J., Chun, M.M. (1997). The fusiform face area: a module in human extrastriate cortex specialized for face perception. *The Journal of Neuroscience: The Official Journal of the Society for Neuroscience*, **17**(11), 4302–11.

Keys, R.T., Taubert, J., Wardle, S.G. (2021). A visual search advantage for illusory faces in objects. *Attention, Perception & Psychophysics*, **83**(5), 1942–53.

Kriegeskorte, N., Mur, M., Bandettini, P. (2008). Representational similarity analysis - connecting the branches of systems neuroscience. *Frontiers in Systems Neuroscience*, **2**, 4.

Landi, S.M., Viswanathan, P., Serene, S., Freiwald, W.A. (2021). A fast link between face perception and memory in the temporal pole. *Science*, **373**(6554), 581–5.

Landi, S.M., Freiwald, W.A. (2017). Two areas for familiar face recognition in the primate brain. *Science*, **357**(6351), 591–5.

Livingstone, M.S., Vincent, J.L., Arcaro, M.J., Srihasam, K., Schade, P.F., Savage, T. (2017). Development of the macaque face-patch system. *Nature Communications*, **8**, 14897.

Mishkin, M., Ungerleider, L.G., Macko, K.A. (1983). Object vision and spatial vision: two cortical pathways. *Trends in Neurosciences*, **6**, 414–7.

Mormann, F., Dubois, J., Kornblith, S., *et al.* (2011). A category-specific response to animals in the right human amygdala. *Nature Neuroscience*, **14**(10), 1247–9.

Morris, J.S., DeGelder, B., Weiskrantz, L., Dolan, R.J. (2001). Differential extrageniculostriate and amygdala responses to presentation of emotional faces in a cortically blind field. *Brain*, **124**(Pt 6), 1241–52.

Nguyen, M.N., Hori, E., Matsumoto, J., Tran, A.H., Ono, T., Nishijo, H. (2013). Neuronal responses to face-like stimuli in the monkey pulvinar. *The European Journal of Neuroscience*, **37**(1), 35–51.

Nguyen, M.N., Nishimaru, H., Matsumoto, J., *et al.* (2016). Population coding of facial information in the monkey superior colliculus and pulvinar. *Frontiers in Neuroscience*, **10**, 583.

Ohayon, S., Freiwald, W.A., Tsao, D.Y. (2012). What makes a cell face selective? The importance of contrast. *Neuron*, **74**(3), 567–81.

Omer, Y., Sapir, R., Hatuka, Y., Yovel, G. (2019). What is a face? Critical features for face detection. *Perception*, **48**(5), 437–46.

Park, S.H., Russ, B.E., McMahon, D.B.T., Koyano, K.W., Berman, R.A., Leopold, D.A. (2017). Functional subpopulations of neurons in a macaque face patch revealed by single-unit fMRI mapping. *Neuron*, **95**(4), 971–81.e975.

Pascalis, O., de Haan, M., Nelson, C.A. (2002). Is face processing species-specific during the first year of life?. *Science*, **296**(5571), 1321–3.

Pitcher, D., Ungerleider, L.G. (2021). Evidence for a third visual pathway specialized for social perception. *Trends in Cognitive Sciences*, **25**(2), 100–10.

Premereur, E., Taubert, J., Janssen, P., Vogels, R., Vanduffel, W. (2016). Effective connectivity reveals largely independent parallel networks of face and body patches. *Current Biology: CB*, **26**(24), 3269–79.

Reid, V.M., Dunn, K., Young, R.J., Amu, J., Donovan, T., Reissland, N. (2017). The human fetus preferentially engages with face-like visual stimuli. *Current Biology: CB*, **27**(12), 1825–8.e1823.

Romanski, L.M., Diehl, M.M. (2011). Neurons responsive to face-view in the Primate Ventrolateral Prefrontal Cortex. *Neuroscience*, **189**, 223–35.

Rossion, B., Taubert, J. (2019). What can we learn about human individual face recognition from experimental studies in monkeys? *Vision Research*, **157**, 142–58.

Sadagopan, S., Zarco, W., Freiwald, W.A. (2017). A causal relationship between face-patch activity and face-detection behavior. *eLife*, **6**, e18558.

Shultz, S., Klin, A., Jones, W. (2018). Neonatal transitions in social behavior and their implications for autism. *Trends in Cognitive Sciences*, **22**(5), 452–69.

Simpson, E.A., Maylott, S.E., Mitsven, S.G., Zeng, G., Jakobsen, K.V. (2020). Face detection in 2- to 6-month-old infants is influenced by gaze direction and species. *Developmental Science*, **23**(2), e12902.

Sugita, Y. (2008). Face perception in monkeys reared with no exposure to faces. *Proceedings of the National Academy of Sciences*, **105**(1), 394–8.

Tamietto, M., de Gelder, B. (2010). Neural bases of the non-conscious perception of emotional signals. *Nature Reviews Neuroscience*, **11**(10), 697–709.

Taubert, J., Apthorp, D., Aagten-Murphy, D., Alais, D. (2011). The role of holistic processing in face perception: evidence from the face inversion effect. *Vision Research*, **51**(11), 1273–8.

Taubert, J., Van Belle, G., Vanduffel, W., Rossion, B., Vogels, R. (2015a). The effect of face inversion for neurons inside and outside fMRI-defined face-selective cortical regions. *Journal of Neurophysiology*, **113**(5), 1644–55.

Taubert, J., Van Belle, G., Vanduffel, W., Rossion, B., Vogels, R. (2015b). Neural correlate of the thatcher face illusion in a monkey face-selective patch. *The Journal of Neuroscience: The Official Journal of the Society for Neuroscience*, **35**(27), 9872–8.

Taubert, J., Wardle, S.G., Flessert, M., Leopold, D.A., Ungerleider, L.G. (2017). Face pareidolia in the rhesus monkey. *Current Biology: CB*, **27**(16), 2505–9.e2502.

Taubert, J., Flessert, M., Wardle, S.G., *et al.* (2018a). Amygdala lesions eliminate viewing preferences for faces in rhesus monkeys. *Proceedings of the National Academy of Sciences of the United States of America*, **115**(31), 8043–8.

Taubert, J., Van Belle, G., Vogels, R., Rossion, B. (2018b). The impact of stimulus size and orientation on individual face coding in monkey face-selective cortex. *Scientific Reports*, **8**(1), 10339.

Taubert, J., Flessert, M., Liu, N., Ungerleider, L.G. (2019). Intranasal oxytocin selectively modulates the behavior of rhesus monkeys in an expression matching task. *Scientific Reports*, **9**(1), 15187.

Taubert, J.Flessert, M., Wardle, S.G., *et al.* (2020a). Amygdala lesions eliminate viewing preferences for faces in rhesus monkeys. *Proceedings of the National Academy of Sciences of the United States of America*, **115**(31), 8043–8.

Taubert, J.Wardle, S.G, Ungerleider, L.G. (2020b). What does a "face cell" want?' *Progress in Neurobiology*, **195**: 101880.

Taubert, J., Parr, L.A. (2012). The perception of two-tone Mooney faces in chimpanzees (*Pan troglodytes*). *Cognitive Neuroscience*, **3**(1), 21–8.

Tsao, D.Y., Freiwald, W.A., Knutsen, T.A., Mandeville, J.B., Tootell, R.B. (2003). Faces and objects in macaque cerebral cortex. *Nature Neuroscience*, **6**(9), 989–95.

Tsao, D.Y., Freiwald, W.A., Tootell, R.B., Livingstone, M.S. (2006). A cortical region consisting entirely of face-selective cells. *Science*, **311**(5761), 670–4.

Tsao, D.Y., Schweers, N., Moeller, S., Freiwald, W.A. (2008). Patches of face-selective cortex in the macaque frontal lobe. *Nature Neuroscience*, **11**(8), 877–9.

Tsao, D.Y., Livingstone, M.S. (2008). Mechanisms of face perception. *Annual Review of Neuroscience*, **31**, 411–37.

Vanduffel, W., Fize, D., Mandeville, J.B., *et al.* (2001). Visual motion processing investigated using contrast agent-enhanced fMRI in awake behaving monkeys. *Neuron*, **32**(4), 565–77.

Visser, R.M., Bathelt, J., Scholte, H.S., Kindt, M. (2021). Robust BOLD responses to faces but not to conditioned threat: challenging the Amygdala's reputation in human fear and extinction learning. *The Journal of Neuroscience: The Official Journal of the Society for Neuroscience*, **41**(50), 10278–92.

Wardle, S.G., Taubert, J., Teichmann, L., Baker, C.I. (2020). Rapid and dynamic processing of face pareidolia in the human brain. *Nature Communications*, **11**(1), 4518.

Wardle, S.G., Paranjape, S., Taubert, J., Baker, C.I. (2022). Illusory faces are more likely to be perceived as male than female. *Proceedings of the National Academy of Sciences of the United States of America*, **119**(5), e2117413119.

Xiang, Q.-S., Ye, F.Q. (2007). Correction for geometric distortion and N/2 ghosting in EPI by phase labeling for additional coordinate encoding (PLACE). *Magnetic Resonance in Medicine*, **57**(4), 731–41.

Yovel, G., Freiwald, W.A. (2013). Face recognition systems in monkey and human: are they the same thing? *F1000prime Reports*, **5**, 10.